Annular flow reactor with side-by-side titania-deposited self-luminous textile and glass fiber velvet for efficient aqueous treatment of active pharmaceutical ingredients

Yige Yan, Frederic Dappozze, Coralie Prevost, Jakub Ederer, Jiří Henych, Sylvie Kříženecká, Maria Humble, Félix Taulou, Laure Peruchon, Jean-Michel Faurie, et al.

Annular flow reactor with side-by-side titania-deposited self-luminous textile and glass fiber velvet for efficient aqueous treatment of active pharmaceutical ingredients

Yige Yan [a, b *], Frederic Dappozze [a], Coralie Prevost [a], Jakub Ederer [c], Jiří Henych [c, d], Sylvie Kříženecká [c], Maria Humble [e], Félix Taulou [f], Laure Peruchon [f], Jean-Michel Faurie [g], Stephane Parola [b *], Chantal Guillard [a *]

[a] *Institut de recherches sur la catalyse et l'environnement de Lyon (IRCELYON), CNRS - Université Lyon 1, UMR5256, 69626 Villeurbanne Cedex, France*

[b] *Laboratoire de Chimie, UMR 5182, ENS de Lyon, 69364 Lyon Cedex 07, France*

[c] *Faculty of Environment, Jan Evangelista Purkyně University in Ústí nad Labem, Pasteurova 3632/15, 40096 Ústí nad Labem, Czech Republic*

[d] *Institute of Inorganic Chemistry, The Czech Academy of Sciences, 25068 Řež, Czech Republic*

[e] *Pharem Biotech AB, Biovation Park, Forskargatan 20J, SE-15136 Södertälje, Sweden*

[f] *Brochier Technologies, 90 Rue Frédéric Fays, 69100 Villeurbanne, France*

[g] *Treffler Production, 290 Rue Ferdinand Perrier, 69800 Saint Priest, France*

* Corresponding authors:

Dr Yige YAN, yige.yan@ircelyon.univ-lyon1.fr

Dr Stephane Parola, stephane.parola@ens-lyon.fr

Dr Chantal Guillard, chantal.guillard@ircelyon.univ-lyon1.fr

Abstract

The release of active pharmaceutical ingredients (APIs) in natural environment has become a global issue. Used as a complementary remediation solution, the heterogenous photocatalysis is underperformed in terms of operation cost per volume of treated wastewater if the non-immobilized catalyst needs to be recovered. This work has identified two promising substrates for the immobilization of TiO_2-based photocatalysts, namely a glass fiber velvet and a self-

luminous textile. The former demonstrated good catalyst attachment and can receive high irradiation intensity from the external UV lamp but required large working volume in the reactor. While the latter suffered from low irradiation intensity delivered by the internal optical fibers, it exhibited high flexibility in shape. Subsequently, a side-by-side combination the above two substrates was implemented in a horizontal annular flow reactor without the need to expand the reactor volume. Using HPLC-MS/MS, ion chromatography, and TOC analysis, the system achieved over 90% degradation of phenol and paracetamol as model pollutants within 60 minutes and an 80% mineralization rate within 120 minutes under laboratory conditions. Furthermore, the system demonstrated cost-efficient degradation of multiple pharmaceutical compounds—achieving 98.3% degradation of caffeine—and a 66% reduction in TOC in a real effluent sample collected from an urban wastewater treatment plant (WWTP) after 360 minutes of treatment, despite the sample's high organic carbon content and elevated inorganic ion concentrations.

Keywords

Photocatalysis, reactor design, active pharmaceutical ingredients self-luminous textile, glass fiber velvet.

1. Introduction

The manufacture and usage of active pharmaceutical ingredients (APIs) are increasingly growing in parallel with the global expansion of healthcare activities. The presence of APIs in water, even at ng/L concentration, has been evidenced or suspected to raise environmental and health concerns. Such concerns include, but not limited to, anti-microbial resistance and hormone disruption effects (behaviour changes, intersex organisms and endocrine related medical conditions). [1] However, as most current wastewater treatment plants (WWTPs) are not specifically designed for the total removal of API residues, [2] the release of APIs into the natural environment has become evident and is now recognized as a global issue. [3] In response, more specific and cost-efficient treatment techniques need to be complemented and further developed to eliminate APIs emissions. Advanced oxidation processes (AOPs) such as UV, ozonation and heterogenous photocatalysis are possible solutions. UV approach suffers from ineffectiveness. [4] The ozonation showed promising results for treating some APIs, yet their applications have been limited by the low solubility of ozone in water and consequent high energy consumption to generate enough ozone [5]. Finally, the heterogeneous photocatalysis might be the most expensive treatment techniques if the catalysts are used in suspension and not being recovered. [6] By consequence, the aforementioned AOPs, in theory, are underperformed compared to homogenous techniques such as Fenton-based process in terms of operation cost per volume of treated wastewater. [7] Among them, the heterogeneous photocatalysis might be converted to one of the most cost-efficient treatment techniques by simply immobilizing the expensive photocatalyst on substrate materials and use them repeatedly. Among the commonly studied photocatalysts today, anatase TiO_2 is still the most cost effective and numerous efforts have been dedicated to the immobilization of TiO_2 on different substrates. For example, TiO_2 nanotubes have been directly anodized on titanium substrate with the presence of fluorinated medium. [8] Moreover, TiO_2 particles can be deposited on functional carbonaceous materials [9, 10] or on micrometric silica-based beads. [6, 11] However, the above immobilization techniques need either sophisticated engineering process or require specific and expensive substrate materials, which prevented them from being used on a large scale.

Glass fiber-based materials are suitable inorganic substrate candidates thanks to the high surface area, low fabrication cost and abundant availability. Furthermore, their excellent thermal stability at high calcination temperatures can allow flexible TiO_2 immobilization procedures. To date, sol-gel-based deposition and subsequent in-situ growth of TiO_2 on woven

glass fiber fabrics have been demonstrated for large surface area applications. [12, 13] Good adhesion is assured by the intimate contact between the precursor sol and the surface of substrate, as well as the post calcination process. However, this method provides insufficient flexibility in control over particle morphology and particle size, which can greatly affect the attachment and photocatalytic performance. In this work, we selected a glass fiber velvet containing numerous protruding fuzzy filaments to increase the total surface area available for contact with TiO_2. Additionally, we aimed to ease the constraints of controlling the morphology of TiO_2 by developing a novel deposition strategy. This approach involves depositing a colloidal suspension of pre-crystallized anatase particles onto the glass fiber velvet, followed by in-situ calcination. Phosphor source was added to the photocatalyst to retain anatase phase and limit the loss of specific surface area during calcination. The superior gas-phase photocatalytic performance of this phosphor- and fluorine-modified anatase nanoparticles has been demonstrated, [14] yet the immobilization of this photocatalyst on glass fiber velvet and the subsequent liquid photocatalytic performance need to be approved.

While the textile-based substrates have been intensively studied for the deposition of TiO_2 as well, [15] we have noticed a unique self-luminous textile substrate. This special textile, provided by Brochier® Technology, [16] is woven from optical fiber and textile yarn. This textile is self-luminous thanks to the build-in optical fibers and is highly flexible in shape. It has been demonstrated that by coating a SiO_2-based layer between textile substrate and TiO_2 layer can simultaneously provide good TiO_2 attachment and prevent optical fiber ageing induced by the photocatalytic activity of TiO_2. [17] Due to the organic nature of the substrate material, deposition of Ti-precursor then post-calcination is not an option. Instead, we used a crystalline anatase photocatalyst obtained by calcinating the commercially Hombikat UV100 TiO_2 for deposition onto the textile substrate. This recently reported easy-to-obtain photocatalyst can effectively degrade phenol, paracetamol and chloramphenicol under laboratory conditions, [18] but the performance under realistic conditions while immobilized has not been evaluated.

In this work, we tried to identify the advantages and weaknesses of the abovementioned two individual substrates. Subsequently, a side-by-side configuration combining both technologies was implemented in a horizontal annular flow reactor in an attempt to realize a cost-effective water treatment solution. First, the individual and combined systems were tested for degradation of two model contaminants: phenol and paracetamol under laboratory conditions. Phenol is a major contaminant whose presence in water can be due to natural

occurrence (dead plants and animals decomposition) or through anthropogenic activities (multiple industrial sectors). [19] Its structure is also quite common in different pharmaceutical chemicals. Paracetamol is a common drug for analgesic and antipyretic uses. [20] Its structure in addition contains nitrogen (as an amide group) in its structure. Finally, an effluent sample collected from an urban WWTP was used to evaluate the efficiency of pharmaceutical compound removal under real-world condition. As a result, an efficient degradation of multiple pharmaceutical compounds has been demonstrated despite high organic carbon content and elevated inorganic ion concentrations using a reactor with modest working volume.

2. Experimental

2.1. Photocatalyst preparation

UV100-700: Commercial Hombikat UV100 TiO_2 was purchased from Sachtleben Chemie GmbH. The UV100-700 photocatalyst was prepared by calcining the UV100 in air with a heating rate of 5 °C·min^{-1} and then kept at 700 °C for 2 h. After cooled to room temperature, the photocatalyst in powder form was used as obtained.

PANaF-700: In a typical sol-gel synthesis for the phosphorus- and fluorine-modified TiO_2 (P/F-modified TiO_2, labeled as PANaF-X, with the X representing the calcination temperature), 5 g of Titanium (IV) isopropoxide (TTiP, Ti(O^iPr)4, 97%, Aldrich) was mixed in 10 g of Propan-2-ol (AnalaR Normapur, > 99.5%, VWR Chemicals), and this solution is labeled as solution A. Then, adequate amount of Sodium fluoride (NaF, ACS reagent, ≥99%, Sigma-Aldrich) and Phosphoric acid (H_3PO_4 (PA), analytical reagent, ≥85%, R.P.Normapur) were added in 6.2 g of 2.2 mol/L acetic acid solution. They provided to the synthesis media the fluoride anion (F^-) and the phosphate anions, respectively. The molar ratio of each additive to titanium was fixed at 0.03, and the obtained solution is labeled as solution B. Finally, the solution B was added dropwise into the solution A. Immediately, a white milky precipitate was formed upon hydrolysis process and the solution was kept under stirring for 1 h, before being further sealed in a glass container and aged at 50 °C for 4 days without any stirring. After filtration of the powder from the rest of the solvent, the solid (labeled as "PANaF") was washed by 2 x 50 mL distilled water for 10 min, before being finally dispersed in 40 ml water for further deposition on glass fiber velvet, this suspension is labelled as suspension C. Part of this suspension was dried at 100 °C and the so-obtained white powder (same as "PANaF") was not

photocatalytically active and was calcined in air at 700 °C for 2 h with a heating rate of 5 °C/min to obtain PANaF-700 in powder form to assess the photocatalytic activity.

2.2. Deposition of TiO_2 on substrates

On Treffler® glass fiber velvet: The glass fiber velvet, supplied by Treffler®, is woven from glass fibers and features numerous protruding fuzzy filaments. It was specifically designed to serve as a catalyst support. [21, 22] The deposition was carried out by coating an aqueous suspension of the already crystallized PANaF particles (suspension C) on the said velvet, followed by an *in-situ* calcination. A functionalization was performed on PANaF particles prior to the deposition. Briefly, 3 ml of Triethanolamine (Sigma, $\geqslant$ 99.0% (GC)) was added in the suspension C and the mixture was kept at 60°C for 30 min in a closed container without string. Then the solid was centrifugated and washed by 2 x 50 mL distilled water for 10 min by cycle. Finally, the ready-to-deposit titania sol was obtained by dispersing the obtained solid in adequate volume of distilled water so that the TiO_2 solid dry weight concentration is 7%. A Triethanolamine-free titania sol was also prepared to study the influence of Triethanolamine on photocatalytic activity of the TiO_2. The titania sol was applied to a 260 mm by 200 mm glass fiber velvet by using a fine painting brush. After drying at 100 °C in a ventilated oven, the deposited velvet was calcined at 700 °C in air for 2 hours with a heating rate of 5 °C·min^{-1}. The glass fiber velvet had been pretreated at 700°C for 2 hours to eliminate any organic sizing prior to the TiO_2 deposition. [23] This pretreatment is to minimize the impact of the organic sizing on the photocatalytic activity of TiO_2. Different types of light source have been coupled with the Treffler® glass fiber velvet to study the impact of the illumination mode on photocatalytic performance. Apart from the tubular UVA lamp, a "veil" composed of polymethyl methacrylate (PMMA) optical fibers woven with monofilament polyester yarn, provided by Brochier®, was selected. Different UVA power input was created by either adjusting the number of connected UVA LEDs, changing the input UVA power of the UVA LEDs or the UVA lamp, or modifying the distance between the “veil” and the velvet.

On Brochier® self-luminous textile: The self-luminous textile was fabricated and provided by Brochier® Technologies. This textile is woven by a combination of polyester textile fiber (Trevira fibers) and PMMA optical fiber interlacely according to the Jacquardloom. The optic fibers are distributed and exposed on the two sides of the textile. Specific treatment was performed on the optical fibers to distribute light emission over the entire surface of the textile [24, 25]. The textile of 260 mm by 200 mm was firstly coated with a layer of SiO_2 by

spraying a SiO_2 sol (Aerodisp W7622). Subsequently, a UV100-700 TiO_2 aqueous suspension was sprayed on both face of the textile. Another deposition method was used to study the impact of the deposition methodology. Briefly, a paste composed of UV100-700 TiO_2 particles was scrapped on the textile surface that has been previously spray-coated with the SiO_2 sol, the latter was then dried at 70 ◦C for 1 h. The minimum deposition quantity of TiO_2 for this method was 19 $mg.cm^{-2}$. The UVA-LEDs with the emission peak centered at 365 nm, was used to connect to the converged optical fiber to deliver the UVA light to the interior of the textile.

Detachment test: Lost rate in weight percentage (w%) of TiO_2 on different substrates compared to the initial TiO_2 weight deposited was accessed to evaluate the adhesion strength of the TiO_2 depositions. Briefly, a 6.3 cm by 20 cm substrate piece was curved and immobilized against the inner wall of a 250 ml beaker, while submerged in 200 ml of distilled water. A magnetic bar was stirring at the bottom center, with its reach close to the surface of substrate without touching it, at 600 RPM for 1 h. Afterwards, the Ti concentration in the water was measured by ICP to deduce the lost quantity of TiO_2. Detachment of TiO_2 from the substrates during photocatalytic test in the annular flow reactor was deduced by analyzing the Ti concentration in the collected outlet flow sample in the end of 360 min (by ICP) in presence of each individual TiO_2-deposited substrate. Two substrates with similar real TiO_2 densities, as measured by ICP, were selected. A TiO_2 density of 3.2 mg/cm^2 was deposited on the self-luminous textile, while the glass fiber velvets had a TiO_2 density of approximately 3.4 mg/cm^2.

2.3. Characterization

Phase identification of dried TiO_2 powders was carried out by X-ray diffraction (XRD) with an Empyrean X-ray diffractometer (Malvern Panalytical) using $CuK\alpha_{1,2}$ radiation in the Bragg-Brentano configuration.

Scanning Electron Microscopy (SEM) observations were performed using a JEOL IT800 scanning electron microscope equipped with In-Lens Schottky Plus Field Emission Election Gun (FEG).

Transmission Electron Microscopy (TEM) analysis was performed using a Philips CM200 in standard mode observation, equipped with thermo-ionic LaB6 filament, operating at a 200 kV acceleration voltage.

ICP-OES analysis was adopted to quantify the Ti density on different substrates. Samples were dissolved in hot HNO_3/HF medium prior to analyses by an Agilent 5800 ICP-OES instrument.

BET surface area of photocatalysts in powder form was measured using a Micrometritics ASAP 2020 system at 77 K with nitrogen sorption. Samples were dried under vacuum overnight at 90 °C prior to the analysis.

A VLX-3W radiometer (from Witec AG) equipped with a sensor specified at 365 nm was used to record UV irradiation at this wavelength on different UV light sources. For the UVA lamp, the record was carried on its center point in length with a 3.6 cm distance between the lamp axis and sensor (half of the annular flow reactor inner diameter). For the self-luminous textile, the irradiance measurements were taken on an uncoated textile sample to assess the irradiation value received by the TiO_2 deposition layer. At a given power input, an average irradiance was calculated by measurements at nine evenly distributed points across the surface (arranged in a 3x3 grid based on the textile's length and width). By default, the sensor surface was positioned in direct contact with the textile during irradiance readings. Calibration of the average irradiance as a function of input current showed a linear dependence over the range of 0 A to 0.9 A. The escaped UVA light through the TiO_2 layer was measured by directly contacting the sensor with the deposited textile surface and the values are relatively low compared to the no-coated counterparts. In a typical case, at a given power input, 3.21 mg/cm^2 of deposited TiO_2 resulted in 0.04 ± 0.04 mW/cm^2 of escaped irradiation compared to 0.36 mW/cm^2 received. The escaped irradiation showed a strong dependency on the measurement positioning, indicating non-uniform deposition across the textile surface. Due to the difficulty in generalizing the non-homogeneous distribution, the escaped irradiation was not subtracted from the received values measured without TiO_2 in this work. A similar approach was applied to the "veil," though with a range of different distances maintained between the "veil" and the sensor.

2.4. Photocatalytic tests

For photocatalysts in powder form. Photocatalytic degradation tests of photocatalysts in powder form were conducted by using a 100 ml Pyrex photo-reactor in air atmosphere. Phenol (99%, Aldrich-Sigma) was used as the model pollutant. For all the experiments, the concentration of the photocatalyst was set to 1 g/L. In detail, 100 mg of catalyst were added to 100 mL of a solution of 20 ppm pollutant with top motorized stirring for 60 min in the dark to reach equilibrium. A pre-heated UV-A PL-L 18W (Philips) was positioned under the reactor. The irradiation at 365 nm measured on the inner bottom side of the reactor was 4.8 mW/cm².

0.8 mL of the solution was sampled and filtrated on an MILLEX HVLP 0.45 μm hydrophilic filter (Millipore, Burlington, MA, USA) for the HPLC analyses.

For TiO_2-deposited substrates. Photocatalytic degradation tests of two types of TiO_2-deposited substrates individually or in combination (side-by-side) were conducted by using a reactor fabricated by Treffler® Production. This reactor is composed of a horizontal annular flow reactor part for photocatalysis treatment, a vertical cylindric reservoir and a pump. The two TiO_2-deposited substrates, both measured of 260 mm by 200 mm, was put in the center of the horizontal annular flow reactor, curved against the outer wall of the reactor. In case of the side-by-side combination, the TiO_2-deposited self-luminous textile was curved and put side-by-side on the outermost side of the TiO_2-deposited glass fiber velvet, against the outer wall of the reactor (Schematic 1 and Schematic S1). A UV-A PL-L 36W U-shape lamp (Philips) was positioned in the center of horizontal annular flow reactor to illuminate the TiO_2-deposited glass fiber velvet. For the TiO_2-deposited self-luminous textile, the optical fibers were grouped into two bundles at one end. These bundles passed through the reactor side wall via sealed holes (sealed with waterproof resin) and were connected to two 3W UVA-emitting LEDs. The length of horizontal annular flow reactor is 423 mm and distance between the perpendicularly connected inlet and outlet is 262.8 mm. The inner diameter of the horizontal annular flow reactor is 72 mm and outer diameter of the inner quartz tube is 40 cm, providing an annular cross-sectional area of 8.04 cm^2. A 2.5 L solution of pollutant at 20 ppm was pumped and internally circulated through the space between the outer wall and an inner quartz tube that protects the center lamp. The flow of the liquid was fixed at 18 L/min. Consequently, the flow speed in the annular space is 37.3 cm/s, and the calculated residence time between the inlet and outlet is 7.05 s. Phenol (99%, Aldrich-Sigma) and paracetamol (99%, Aldrich-Sigma) were used as model pollutants.

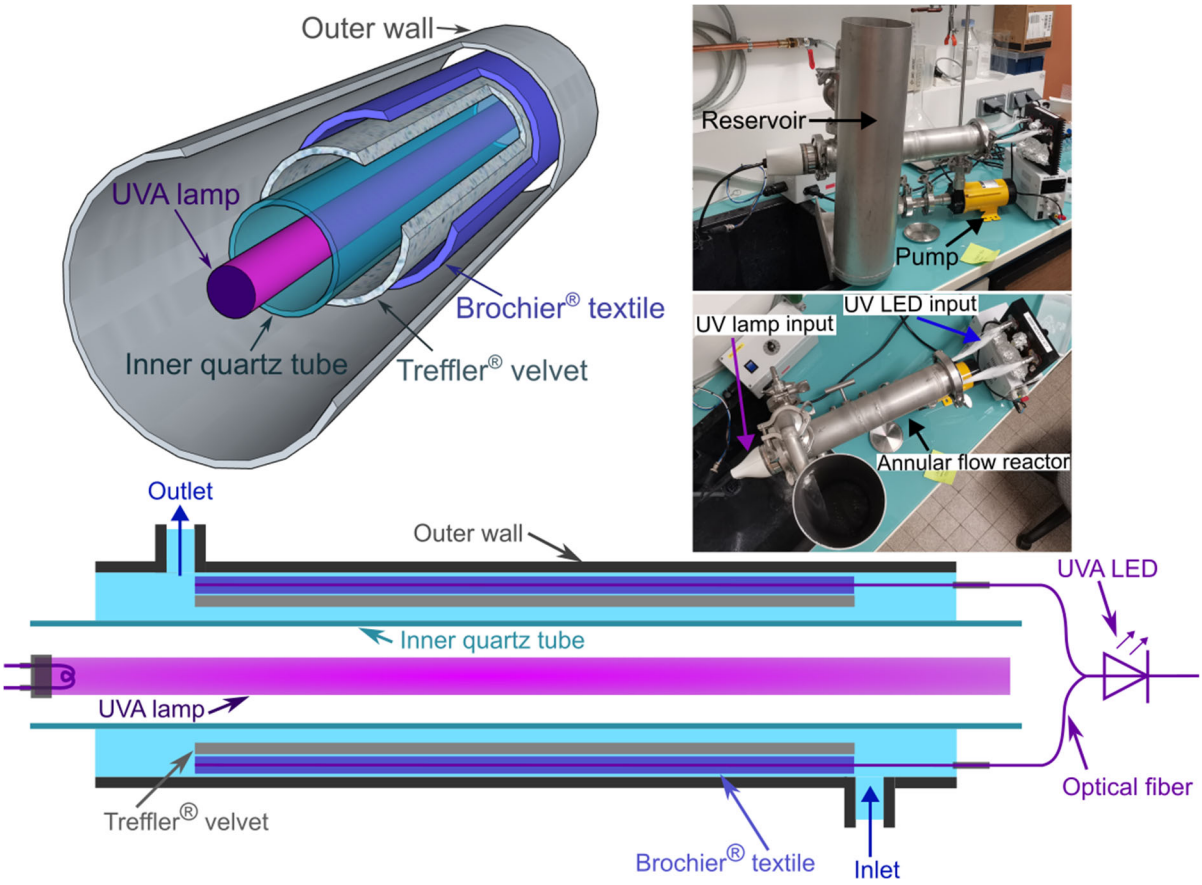

Schematic 1. Side-by-side combination of two substrates, namely Treffler® glass fiber velvet and Brochier® self-luminous textile, in a horizontal annular flow reactor in 3D perspective and in cross-section side view, along with the photos of the real appearance (including reservoir and pump parts).

To access the photocatalytic performance in remediating pharmaceutical compounds under real-world conditions, we used a disc-filtered effluent water that was obtained from the company SYVAB in Sweden. SYVAB operates the Himmerfjärden WWTP, which receives wastewater from the southern Stockholm region. At SYVAB, the wastewater is treated using mechanical treatment, biological purification and finally disc filtration (10 µm) before it is released into the Baltic Sea. More information on how SYVAB treats wastewater and treatment results can be obtained at their website (www.syvab.se). The effluent water was collected after the disc filter (which means that the water is ready to be released to the sea) in a plastic can and was sent to France to conduct the photocatalytic tests. The received effluent sample was autoclaved at 125 °C for 20 min and stored in a fridge to avoid excessive microorganism development prior to tests. 2.5 L of effluent was used in each photocatalytic treatment. During the test; 7 mL of the solution was sampled at each measurement point and filtrated on an

MILLEX HVLP 0.45 µm hydrophilic filter (Millipore, Burlington, MA, USA) for the HPLC and TOC analyses.

HPLC analyses for phenol and paracetamol were performed using a Shimadzu system (Shimadzu, Japan) equipped with a photodiode array detector and a 150 mm × 4.6 mm x 2,7µm-Ascentis Express 90 Å AQ-C18 column (Supelco Merck). The mobile phase was a 95 %v / 5%v acidified Water (with 0.1%w/w HCOOH) / Methanol mixed solution. In all cases the flow rate was set at 1.0 mL/min. All of the HPLC analysis were performed at 40 °C.

Ionic chromatography was used to trace the concentration of NH_4^+/NO_3^- in model pollutant molecule that contains nitrogen atoms. The instrument was a Metrohm 881 Compact IC pro. Two columns, thermostated at 30 °C, were used: Metrosep C4 150/4.0 for cations and Metrosep A supp5 150/4.0 for anions. The mobile phases were mixtures of both 1.7mM nitric acid and 0.7mM of dipicolinic acid for cations, and of 3.2mM sodium carbonate and 1mM sodium hydrogenocarbonate for anions. Both flow rates were set at 1.0 mL/min. Conductivity detector suppression was made by a 0.1M Phosphoric acid solution.

The analysis of inorganic anions in the real effluent was performed using an ion-exchange chromatography system (DIONEX ICS 1000) equipped with a conductivity detector. A Dionex IonPac™ AS22 column (4x250 mm) was used for the separation of anions. The mobile phase consisted of 4.5 mM Na_2CO_3 and 1.4 mM $NaHCO_3$, with a flow rate of 1.2 ml/min. The samples were measured directly without further purification or dilution, and the effluent water samples were only filtered using 0.2 µm PTFE syringe filters. The concentration of inorganic anions was determined using previously measured calibration curves.

The pharmaceutical compounds in the real effluent sample were analysed using an Agilent 1290 Infinity II UHPLC system (Agilent Technologies). Chromatographic separation was achieved using a Luna Omega PS C18 analytical column 2.1x100 mm, 3 µm particle size from Phenomenex at a flow rate of 0.4 ml/min. The mobile phases consisted of (A) H_2O with 0.5 mM NH_4F + 0.01% HCOOH and (B) acetonitrile + methanol (1:1). The gradient was 90% A at 0 min, 0% A at 6 min to 8 min, 90% A at 8.1 min. The post time was 3.9 min with 90% A and the stop time 11 min. The HPLC system was coupled to an Agilent G6495A Triple Quadrupole mass spectrometer equipped with an Agilent Jet Stream electrospray ionization source. Agilent MassHunter Acquisition software was used for data acquisition, and Agilent MassHunter Workstation software was used for data analysis. The samples were filtered using 0.2 µm PTFE syringe filters and diluted accordingly depending on the concentration of specific target molecule.

Reaction rate constant for the first order decay kinetics was calculated by the formula:

$$\frac{[A]_{1/2}}{[A]_0} = \frac{1}{2} = e^{-kt_{1/2}} \quad (1)$$

Where $[A]_0$ is the initial concentration of the molecule A after absorption period in the dark, $[A]_{1/2}$ is the concentration of $[A]_0$ decreased by half, $t_{1/2}$ is the timescale on which the initial concentration $[A]_0$ is decreased by half. K is the reaction rate constant presented in min^{-1}.

The Total Organic Carbon (TOC) of all samples was quantified using a Shimadzu TOC-VSCH model equipped with an autosampler. The detection limit of the TOC analyzer is 0.5 mg/L and the quantification limit is 1 mg/L. The curve of TOC as function of time were fitted using Origin® software by the Boltzmann sigmoid formula:

$$y = A_2 + \frac{A_1 - A_2}{1 + e^{(x-x_0)/dx}} \quad (2)$$

Where A_2 is the final value, A_1 is the initial value, x_0 is the inflection point (where the plot curvature changes), dx is the time constant. To help location the inflection point, 1st derivative of TOC as a function of time was plotted against the time. The inflection point is where the latter curve reaches its minimum.

3. Results and discussions

3.1. Choice of photocatalysts on different substrates

The Brochier® textile is intricately woven by polymer-based textile fiber and optical fiber, which impose two restrictions on the deposition of TiO_2. First, an *in-situ* crystallization of TiO_2 by calcinating a deposited organic Ti precursor cannot be realized, as the textile is not designed to sustain high temperature treatment. Thus, only crystallized TiO_2 can be deposited without calcination. Secondly, the photocatalytic oxidative property of the crystallized TiO_2 can self-damage the textile surface, accompanied by a rapid deterioration of light distribution efficiency. A protection measure on textile must be envisaged. To overcome these two restrictions, highly crystalline anatase TiO_2 particles were first produced by calcining the commercial Hombikat UV100 at 700 °C (namely UV100-700), then they were deposited on textile surface that was covered by a layer of silica sol. The silica sol can bind TiO_2 particles and simultaneously protect organic fiber from intimate contact with TiO_2 particles, thus can significantly limit the photocatalytic aging of the organic fibers [17]. The selection of this photocatalyst is based on a recent study [26] on its high photocatalytic activity in the phenol, paracetamol and

chloramphenicol degradation, which is likely due to the high crystallinity of the anatase phase (the only existing phase, Figure 1a) resulting from high temperature calcination of the commercial Hombikat UV100, aided by the self-contained sulfur's retarding effect on the anatase-to-rutile transition. The specific surface area of UV100-700 catalyst is about 18 m^2/g (Table 1) and the mean crystallite size calculated from the XRD pattern is about 23.6 nm.

The Treffler® velvet, woven from glass fibers, allows for the deposition of a Ti precursor followed by an *in-situ* calcination process. Instead of using an organic Ti precursor, we opted for a pre-crystallized TiO_2 suspension, to achieve a better control over the crystallinity and particle morphology evolution during the post-calcination step. In detail, we have deposited a dispersible titania sol, consisting of pre-crystallized TiO_2 modified with phosphorus (P) and fluorine (F) by sol-gel route, on the velvet surface and followed by an *in-situ* calcination at 700°C. This photocatalyst, labeled as "PANaF-X (X is the calcination temperature)" has demonstrated superior gas-phase degradation performance for butane-2-one after calcination. [14] The enhanced photocatalytic activity can be attributed to the high anatase crystallinity and the high surface area of this catalyst thanks to the roles of phosphorus in suppressing particle growth and delaying the anatase-to-rutile phase transition during calcination. Additionally, the more controlled anatase crystallization kinetics during the sol-gel synthesis promoted by phosphorus and the increased exposure of the active {001} facet due to fluorine's structuring effect also contributed to the enhanced photocatalytic activity. Indeed ,the photocatalyst deposited on the velvet can still retain a moderate specific surface area of 63 m^2/g and a small crystallite size of 14 nm after calcination at 700°C, compared to 131 m^2/g and 11 nm before calcination (Table 1, Figure 1a and Figure S1). These properties, along with the high specific surface area and excellent dispersibility of the TiO_2 particles, allow for extensive contact with the glass fibers, improving the physical interaction and adhesion strength of the photocatalyst to the velvet. Calcination is necessary since the non-calcined PANaF TiO_2 showed no noticeable photocatalytic activity (not shown).

Table 1. Summary of main characterizations and photocatalytic phenol degradation rate constants of different TiO_2 photocatalysts that would be used on different substrates.

Sample	Specific surface area (m^2/g)	Mean crystallite size (nm)	Phenol decay rate constant (min^{-1})
PANaF-700	63	13.6	0.019
UV100-700	18	23.6	0.017

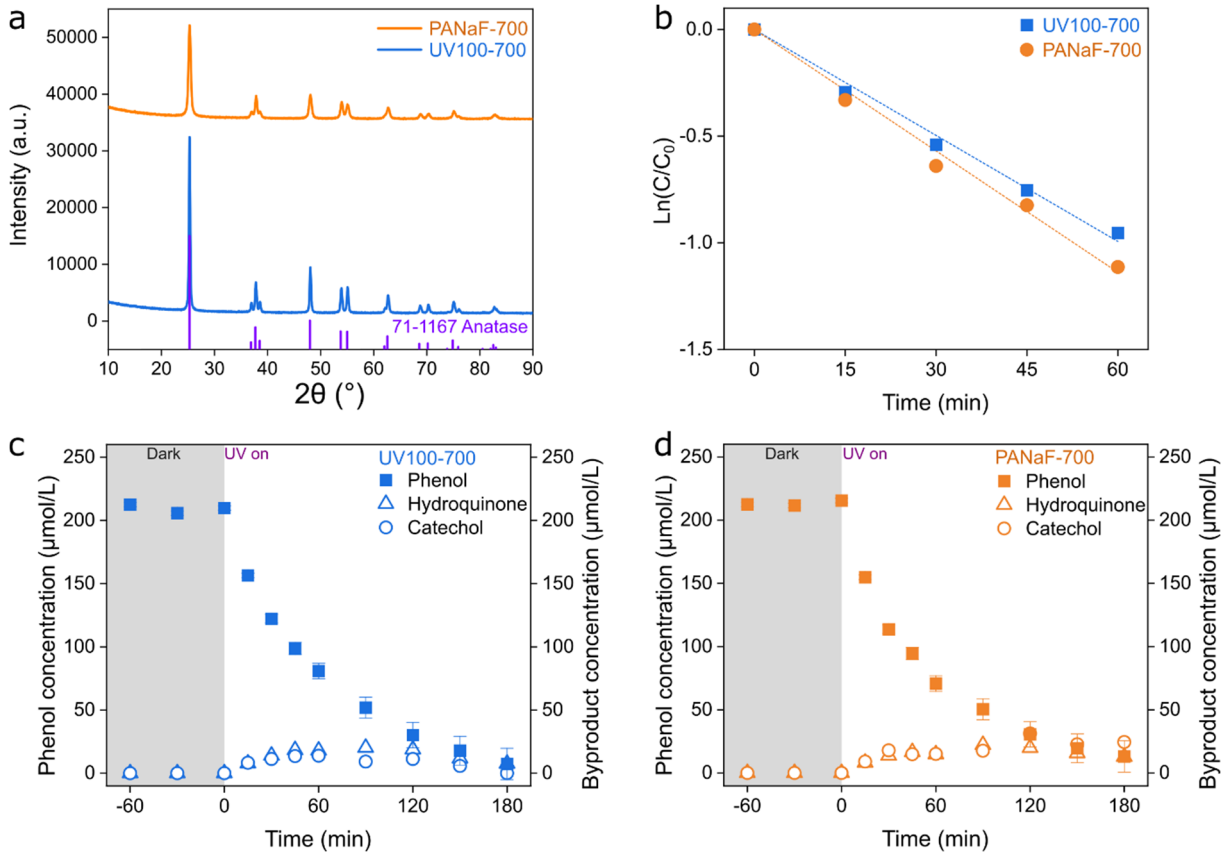

Figure 1. (a) XRD patterns of TiO_2 UV100-700 and PANaF-700 in powder form. Anatase reference pattern is included at the bottom. (b) $Ln(C/C_0)$ of photocatalytic phenol degradation plotted against the irradiation time for UV100-700 and PANaF-700 in powder form, the slope of curve is defined as -k (min^{-1}). (c-d) Concentration of phenol and generated hydroquinone and catechol concentration as a function of time in presence of UV100-700 and PANaF-700 in powder form. The initial concentrations of phenol were targeted to 20 ppm in weight, equivalent to 212.5 µmol/L. All curves have been normalized so that the phenol concentration at Time = -60 min is 212.5 µmol/L.

Liquid-phase photocatalytic performance of these two photocatalysts in powder form were compared. Phenol degradation and generation of Hydroquinone and Catechol as intermediate degradation products were followed (Table 1 and Figure 1b-d). Both photocatalysts exhibited similarly efficient degradation rate during the 3 hours of illumination time. A balanced trade-off between specific surface area and anatase crystallinity, influenced by the effects of sulfur or phosphorus in retarding crystallization kinetic, [27] achieved through carefully controlled calcination temperature, might account for their similarly high photocatalytic activities. Thus, the intrinsic photocatalytic activity of the different catalysts will be a neglected factor for the following parts of the work after they are deposited on different substrates.

3.2. Parameter studies on individual substrates

An average of 35% by weight of UV100-700 photocatalyst can be efficiently deposited on Brochier® self-luminous textile by spray method when the real TiO_2 weight density reached approximately 3 mg/cm^2 (Figure 2a, e-f) (Figure S2 and Figure S3). The low surface area, large crystallite size and high degree of particle aggregation of this photocatalyst (Figure S4) have limited the attachment strength on the textile, specifically on top of the silica layer. Once the thickness of TiO_2 deposition layer surpassed a certain threshold, the binding effect from the silica layer can no longer cover the TiO_2 layer in excess. On the other hand, about 65% by weight of UV100-700 photocatalyst can be efficiently deposited by scraper method (Figure 2a and Figure S2). This method relies on the densely compacted TiO_2 particles to deliver the attachment force. However, a minimum processable quantity of 13 mg of TiO_2 per cm^2 is required, as the spreading of the highly concentrate TiO_2-containing paste over the entire textile surface would become difficult below this threshold. The degradation rate constants for phenol increased with the real deposited TiO_2 density when the total surface area of the textile was fixed (Figure 2b). The high deposited amount of TiO_2 by scraper method did not lead to further increase in the degradation rate constant. Naturally, excessive layer of the deposited TiO_2 cannot receive sufficient UV irradiation coming from the inside of the self-luminous textile. Although the scraper method resulted in more efficient TiO_2 deposition, its high minimum deposition threshold and low photocatalytic performance per TiO_2 quantity ratio have reduced the overall cost-effectiveness value. Consequently, this method will not be pursued in further studies. The degradation rate constants for phenol have expectedly increased with the surface area of the textile when the real deposited TiO_2 density was fixed (Figure 2c). Finally, the degradation rate constants for phenol also increased with the received irradiation up to a rate constant of approximately 0.053 min^{-1}, before the value approached a pseudo-plateau (Figure 2d). Considering that the irradiation originates from optical fibers embedded within the TiO_2 deposition, we believe that an irradiation intensity of 0.35 mW/cm^2 is sufficient to penetrate the entire thickness of the TiO_2 layer at around 3 mg/cm^2. The TiO_2 particles deposited closest to the optical fiber likely contributed the most to the photocatalytic activity, while the outer layer of TiO_2, which received significantly less UV light, made less contribution.

During the detachment test, 0.39% of the weight of the photocatalysts has been lost in contact with a strong water current when the real TiO_2 density was about 3.2 mg/cm^2, showing the robust adhesion of TiO_2 on the silica sol (Table S1).

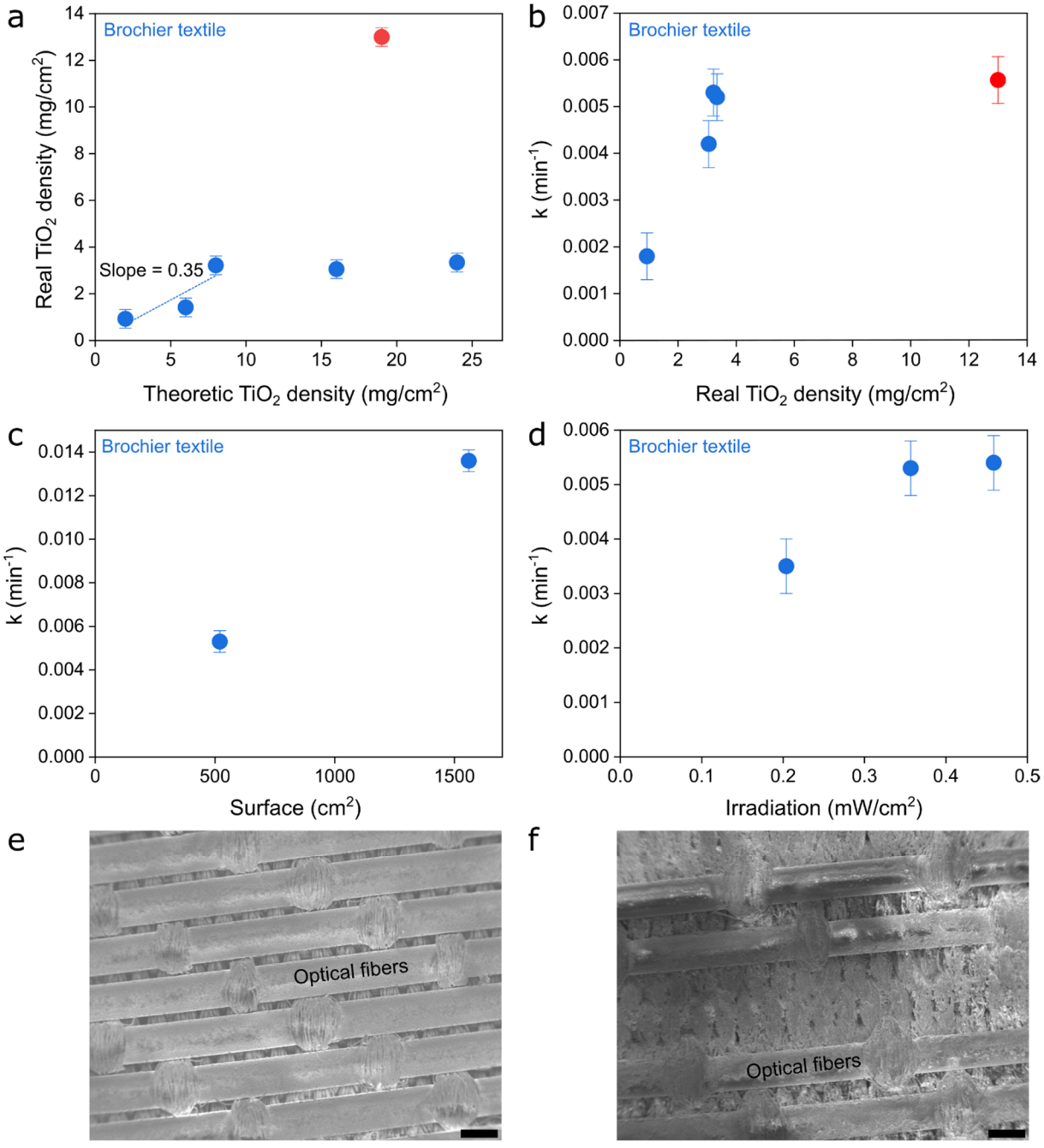

Figure 2. (a) The relationship between the theoretical and real TiO_2 deposited on Brochier® self-textile by spray and scraper methods. The blue spheres represent spray method, the red sphere represents scraper method. (b) Phenol degradation rate constant k (min^{-1}) as a function of the real TiO_2 density deposited on the Brochier® textile. The blue spheres represent spray method, the red sphere represents scraper method. The UVA irradiation (at 365 nm) was about 0.36 mW/cm^2. (c) Phenol degradation rate constant k (min^{-1}) as a function of the surface area of the Brochier® textile. The real TiO_2 density deposited was about 3.2 mg/cm^2 and the UV irradiation was about 0.36 mW/cm^2. (d) Phenol degradation rate constant k (min^{-1}) as a function of the UV irradiation (at 365 nm). The surface area of the Brochier® textile is fixed at 520 cm^2 and the real TiO_2 density deposited was about 3.2 mg/cm^2. (e) SEM image of

438 the uncoated Brochier® textile. (f) SEM image of the Brochier® textile deposited with about 3 mg/cm^2
439 of TiO_2. The scale bars in (e) and (f) are 500 μm.
440
441 For the Treffler® glass fiber velvet, the deposition of a pre-crystallized anatase TiO_2 sol
442 ("PANaF", Figure S5) followed by calcination has resulted in an average weight deposition
443 efficiency of 41% when the real TiO_2 weight density reached approximately 3.4 mg/cm^2 (Figure
444 3a). The degradation rate constant for phenol, if other parameters were fixed, has rapidly
445 reached near 0.02 min^{-1} at a real TiO_2 deposition density of about 1.2 mg/cm^2 and this value
446 has marginally increased to about 0.023 min^{-1} when the TiO_2 deposition density was further
447 increased to 3.2 mg/cm^2 (Figure 3b). At 1.2 mg/cm^2, the rate constant may have reached a
448 pseudo-plateau. The TiO_2 deposited on the tips of the glass fiber filaments in the front layer of
449 the velvet could obstruct the penetration of UVA light to the bottom layer. As expected,
450 excessive TiO_2 deposition would lead to limited performance improvement. The coverage of
451 TiO_2 on the surface of the glass fibers has been observed in SEM images (Figure 3c-d and
452 Figure S6).
453 The deposition of a triethanolamine-functionalized PANaF TiO_2 particles on velvet
454 followed by calcination has greatly decreased the photocatalytic performance on the
455 degradation of phenol compared to the triethanolamine-free counterpart if other parameters
456 were fixed (Figure S7a). We attribute the decreased photocatalytic activity to the excessive
457 insertion of nitrogen atoms into the TiO_2, which could compromise the crystallographic
458 integrity of the anatase phase or create an abundance of detrimental electron traps. [28] Even
459 after calcination at 700 °C for 2 hours, the velvet coated by using Triethanolamine-
460 functionalized PANaF TiO_2 retains a yellowish color, indicating the thermal stability of the
461 inserted nitrogen atoms (Figure S7b).
462 A study on the photocatalytic performance with different modes of light sources has
463 revealed a linear dependence of the phenol degradation rate constant as a function of the
464 received UVA irradiation (Figure S8). By far, the UVA lamp is the most optimal option because
465 of its high UVA irradiation emitted.
466 During the detachment test under a strong water current at a given real TiO_2 deposition
467 density (approximately 3.4 mg/cm^2), 0.66% by weight of the triethanolamine-functionalized
468 PANaF TiO_2 photocatalysts was lost, compared to a loss rate of 1.66% for the triethanolamine-
469 free counterpart (Table S1). Although triethanolamine has improved the attachment of TiO_2 on
470 the glass fiber velvet, the improvement was relatively limited. We attributed the strong adhesion

primarily to the high surface area and good dispersion properties of the PANaF TiO_2 particles, which created an intimate contact with the glass fiber filaments, further reinforced by the *in-situ* calcination. Therefore, only triethanolamine-free PANaF TiO_2 particles will be used for deposition on glass fiber velvets, considering the balance between photocatalytic performance and attachment stability.

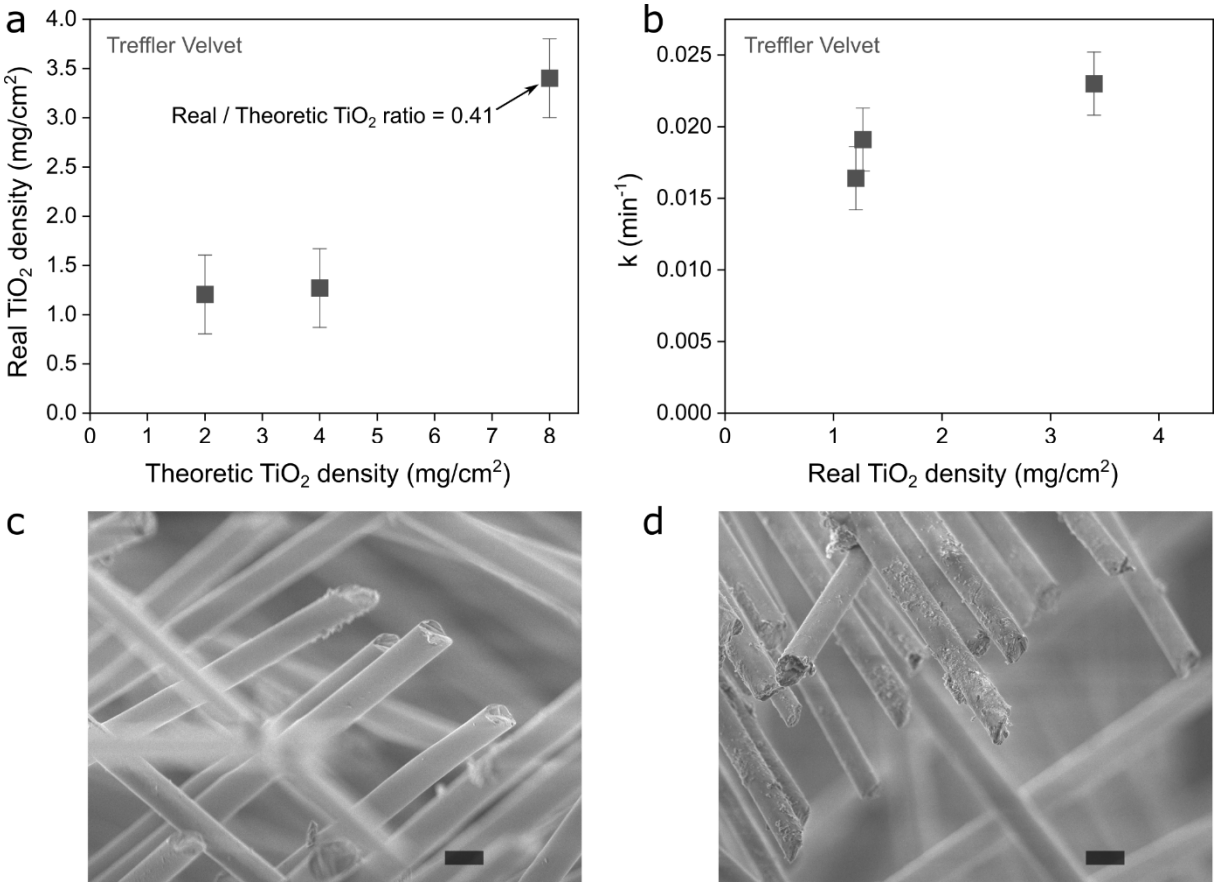

Figure 3. (a) The relationship between the theoretical and real TiO_2 deposited on Treffler® glass fiber velvet by deposition of PANaF TiO_2 sol followed by *in-situ* calcination. (b) Phenol degradation rate constant k (min^{-1}) as a function of the real TiO_2 density deposited on the velvet. The UVA irradiation (at 365 nm) was about 4.05 mW/cm^2. In (a-b), the trend lines (dotted lines) pass zero point. (c) SEM image of the uncoated Treffler® glass fiber velvet. (d) SEM image of the Treffler® glass fiber velvet deposited with about 1.2 mg/cm^2 of TiO_2 (without usage of triethanolamine) and after calcination at 700 °C for 2h. The scale bars in (c) and (d) are 10 μm.

3.3. Side-by-side combination of the two substrates

Typically, in a annular flow reactor for liquid-phase photocatalysis, a large volume is occupied by the interval space separated between the catalyst surface and the central UV lamp. The liquid flows within this space to come into contact with the catalyst while letting the light

source to reach the catalyst surface. As the light is mostly absorbed (blocked and stopped) by the TiO_2-deposited substrate, any space that is left behind the substrate (on the opposite side of the lamp), if existed, is basically useless. By consequence, the use of an excessively large substrate that leads to over-rolling is meaningless. By our side-by-side combination configuration, the self-luminous Brochier® textile can utilize the outermost space behind the Treffler® glass fiber velvet (which is illuminated by the central lamp) thanks to the self-supplied UV source and the flexibility of this textile. As a result, there is no need to expend the reactor size (Schematic 1 and Schematic S1).

To demonstrate the advantage of the combination of two substrates, photocatalytic degradation of two model pollutant molecules, phenol and paracetamol (Figure S9), has been performed individually on each substrate and jointly with the side-by-side presence of the two substrates. Photocatalytic degradation rate of the model molecules, generation of by-products and the total organic carbon were followed with time, and the results are presented in Table 2 and Figure 4. With identical substrate area, similar deposited TiO_2 density and similar irradiance, the two individual substrates exhibited similar phenol degradation rate constant (Figure S10). Therefore, as expected, the glass fiber velvet showed a much more efficient oxidation of phenol and paracetamol compared to the self-luminous textile only because the former has received much more UV irradiation from the UVA lamp.

The side-by-side combination system has resulted in a disappearance of phenol in 120 min of illumination time (Figure 4a). Hydroquinone and Catechol were quickly generated, then disappeared before 120 min after reaching to a turning point between 30-50 min (Figure 4c). This turning point is coherent to the inflection point of TOC curve fitted by Sigmoidal model and its derivative (48.5 min, Table 2, Figure 4e and Figure S11). These observations aligned with the fact that the photocatalytic degradation of phenol consisted of hydroxylation at early stage of the reaction without carbon mineralization, and aromatic ring opening and oxidation of hydrocarbon species into CO_2 were not the main reaction pathway until the inflection point.

Paracetamol undergoes successive long photocatalytic degradation steps before being mineralized into CO_2 as well as into NH_4^+/NO_3^-. Identifying and quantifying a full list of organic intermediate molecules for the degradation of this pollutant are not the goal of this paper, readers can refer the works done by Yang *et al.* [29] for this purpose. We are interested in the original molecule decay rate and the mineralization yield. The combined system has resulted in a rapid degradation of paracetamol to near total disappearance short after 60 min of irradiation (Figure 4b). The nitrogen mineralization rate is around 76% at a reaction time of 240

min (Figure 4d). The TOC curve exhibited a fast inflection point at about 29 min, but has reached a plateaued mineralization rate about 81% mineralization at 240 min of irradiation (Figure 4f). It seems that the photocatalytic oxidation of paracetamol was generally fast, but became difficult in degrading small molecule(s) containing both carbon and nitrogen at the end of the degradation pathway. Among the end degradation products, we have excluded Acetamide, Maleic acid, Fumaric acid, oxalic acid and acetic acid by HPLC calibration and have hypothesized that formamide might be formed but were unable to confirm it yet.

The experimentally obtained degradation curves of phenol and paracetamol for the combined system were very similar with those simulated by mathematically superimposing the two degradation curves of individual system (Table 2, Figure 4a-b and Figure S12). Although it is unpractical to precisely compare them quantitatively due to the lack of data points and the error marge (Table S2), a good additive effect on the degradation of model molecules has been demonstrated in terms of the internal and external energy specific degradation rate constant total input energy by the side-by-side combined substrates (Table S2). We can confidently rule out the theory suggesting that water flow obstruction or restricted molecular diffusion is caused by substrate overlap within the confined space of the reactor.

The detachment of TiO_2 photocatalysts by the flow in the annular flow reactor was accessed by analyzing the Ti content in the collected outlet flow sample at the end of 360 min of reaction time (Table S1). Both substrates demonstrated good TiO_2 adhesion strength in our condition by losing less than 0.1 % of TiO_2 weight in a flow rate of 18 L/min. Although a few sediment particles were detached from the TiO_2-deposited textile (Figure S13), they are large enough to resist the current. No detached particle from TiO_2-deposited velvet has been noticed by visual observation in the flow (Video S1).

Table 2. Table of results of individual or side-by-side combination of the two substrates on photocatalytic phenol and paracetamol degradation.

[a] Internal energy specific degradation rate constant is the degradation rate constant divided by the received UVA energy (at 365 nm).

[b] Phenol, [c] Paracetamol

Sample	Area (cm^2)	Real deposited TiO_2 ($mg.cm^{-2}$)	Received irradiation at 365 nm ($mW.cm^{-2}$)	Degradation rate constant k (min^{-1})		Internal energy specific degradation rate constant ($min^{-1}.W^{-1}$) [a]		TOC			
				Phe.[b]	Para.[c]	Phe.	Para.	Inflection point		Time constant	
								Phe.	Para.	Phe.	Para.
Textile only	520	3.2	0.36*2	0.004	0.006	0.011	0.015	201.1	229.7	93.7	163.6
Velvet only	520	3.5	4.01	0.017	0.017	0.008	0.008	79.9	56.9	41.4	45.9
Combined (Exp)	-	-	-	0.031	0.042	0.013	0.017	48.5	29.8	24.4	31.3

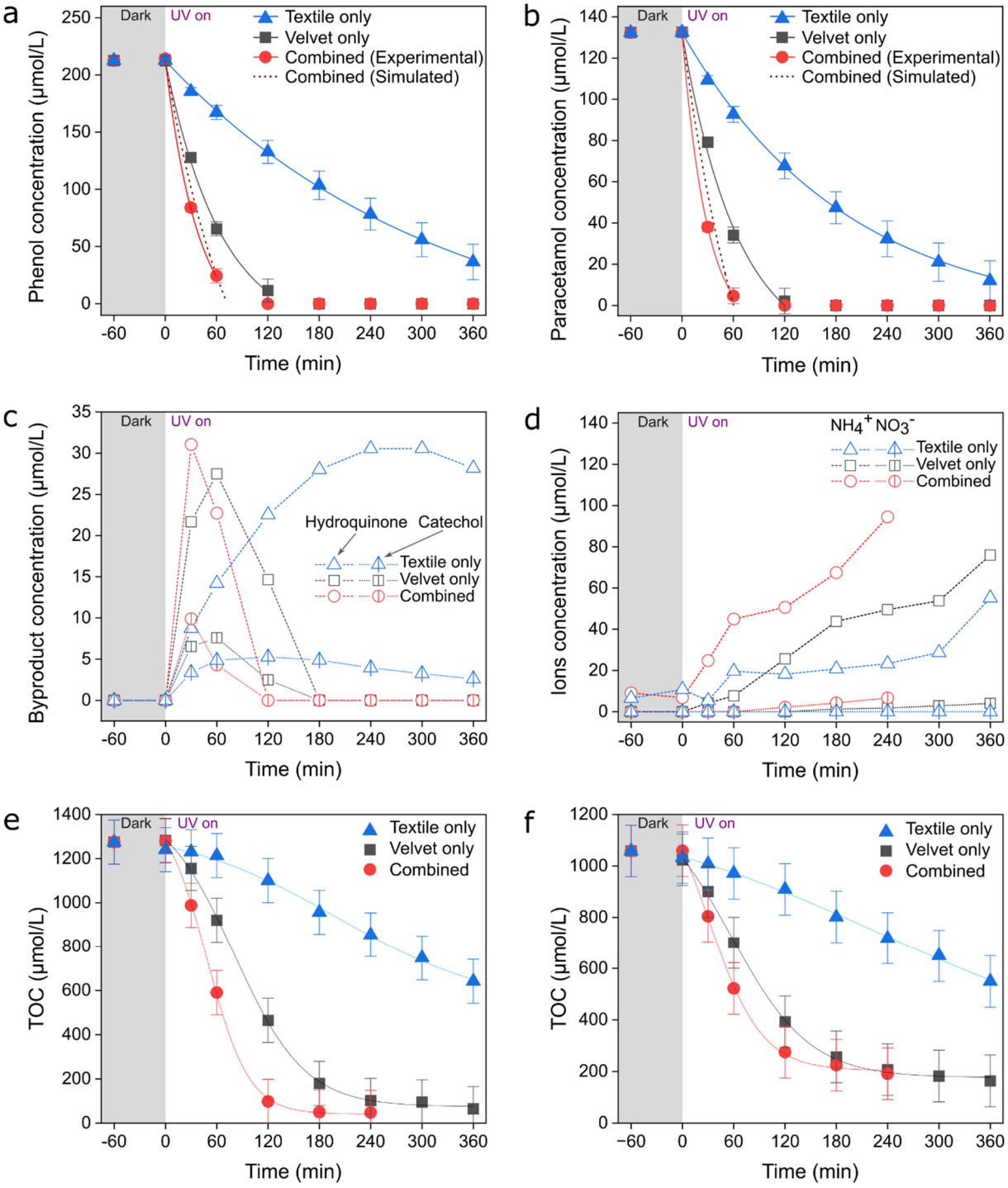

Figure 4. Degradation rate constant k (min^{-1}) of (a) Phenol and (b) Paracetamol as a function of illumination time in presence of Brochier® textile or Treffler® velvet or the side-by-side combination of two substrates. The initial concentrations of phenol and paracetamol were targeted to 20 ppm in weight, equivalent to 212.5 µmol/L and 132.3 µmol/L respectively. All curves have been normalized so that the phenol and paracetamol concentration at Time = -60 min is 212.5 µmol/L and 132.3 µmol/L respectively. Simulated degradation curves for the combined system are obtained by mathematically superpositioning the two individual degradation curves. Concentrations of (c) Hydroquinone and Catechol formation from the degradation of phenol nitrate and those of (d) ammonium and nitrate ions from degradation of paracetamol are plotted as a function of illumination time in presence of individual or combined substrates. TOC curves of the concentration of carbon remaining in the liquid medium are plotted as a function of illumination time for the degradation of (e) Phenol and (f) Paracetamol in presence of individual or combined substrates.

3.4. Real effluent

The horizontal annular flow reactor with side-by-side combination of TiO_2-deposited self-luminous textile and glass fiber velvet has been employed to treat a real urban WWTP effluent sample. Traces of various pharmaceutical compounds have been detected (Table S3 and Figure S14). It's important to note that the exact composition of organic and inorganic compounds in the effluent may fluctuate over time, influenced by the collection location, pharmaceutical production activities and seasonal variations. In this particularly effluent sample, the sum of organic carbon concentration of all detected pharmaceutical compounds is about 1.5 μmol/L compared to about 950 μmol/L for the total organic carbon (TOC). It is in line with our expectation that the pharmaceutical compounds existed in trace level and were accompanied by large quantity of unknown organic compounds. Molecular concentrations of pharmaceutical compounds before and after 360 min of photocatalytic treatment and TOC curves of the individual and the combined system as a function of irradiation time are shown in Figure 5a-b and Figure S15. The velvet, as expected, was much more effective than textile due to the more abundant UV irradiation received, and the combined system has resulted in efficient elimination of both pharmaceutical compounds as well as a rapid decay of TOC value (about 66% of TOC reduction). Although the pharmaceutical compounds represented a small portion of the organic compounds, they were relatively well degraded (Figure 5c). Notably amount them, Caffeine was the main pharmaceutic compound and has been reduced by 98.3%; while most of others (*e.g.*, Gabapentin, Meteprolol, etc.) have been reduced to their detection limits after 360 min of treatment except paracetamol, whose concentration was increased in the more efficient systems (i.e., on velvet and combined systems). No compound among the given list is known to degrade into paracetamol under normal circumstances, since their chemical structures differ significantly from that of paracetamol. However, it is possible that during photocatalytic degradation processes in a chemical environment rich in unknown organic compounds, some unexpected degradation intermediates could form.

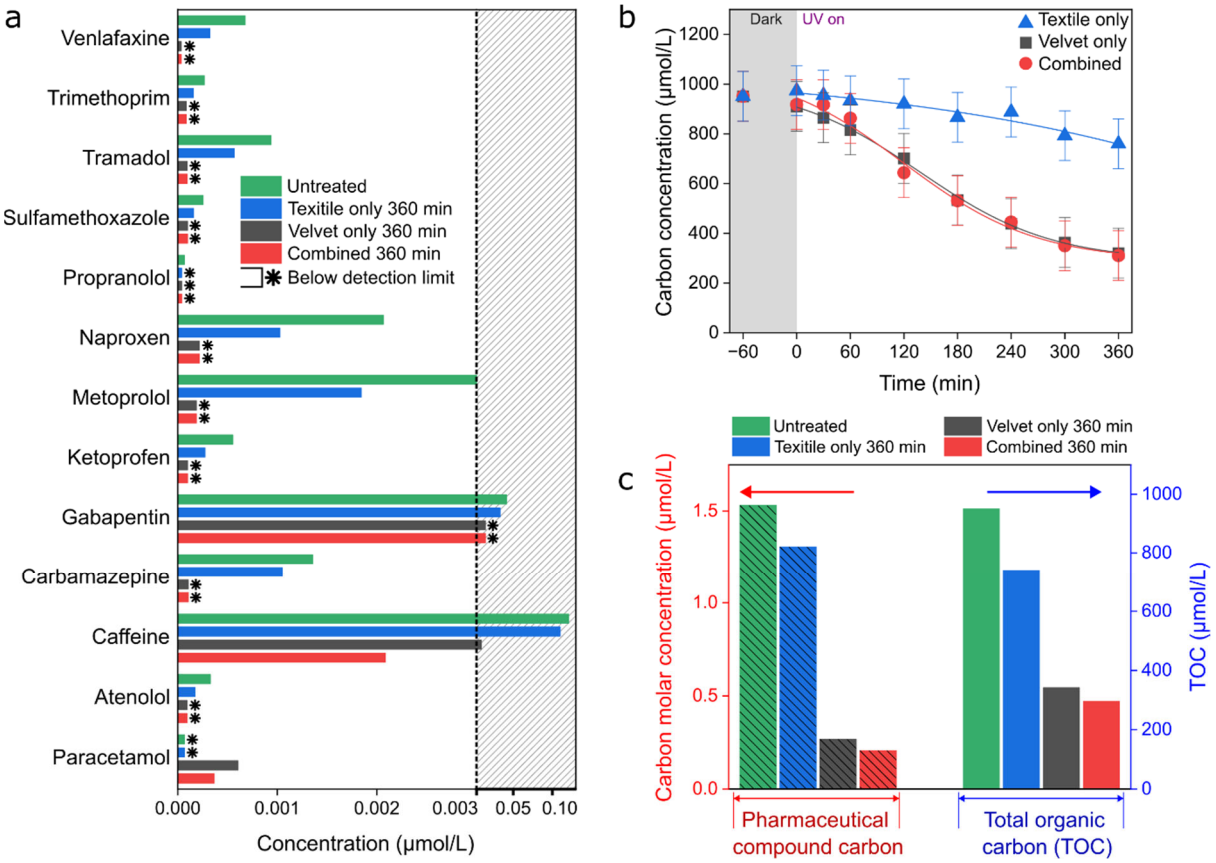

Figure 5. (a) Molecular concentrations of pharmaceutical compounds in the real effluent before and after 360 min of photocatalytic treatment by individual and the side-by-side combined system. The patterned zone is in a larger scale than the non-patterned zone. (b) TOC curves of the real effluent treated by individual and the combined system as a function of irradiation time. (c) Comparison of the sum of carbon concentrations of pharmaceutical compounds and TOC concentrations in the real effluent before and after 360 min of photocatalytic treatment by individual and the combined system.

The UV-Vis spectra of the effluent showed a dominant absorption intensity at < 250 nm, a peak around 265 nm and gradually diminished absorption beyond (Figure 6a). The photocatalytic treatment led to a decreased absorption most significantly between 250 nm and 400 nm, while the evolution of those below 250 nm has been less noticeable. Figure 6b showed UV-Vis absorption value at a specific wavelength between 205 to 450 nm of the effluent during the photocatalytic treatment as a function of time by individual or combined systems. The deposited velvet and the combined system led to rapid and efficient decrease in absorption especially between 250 to 350 nm after 360 min of treatment. On the other hand, the absorption values below 220 nm were also recorded. Their absorption values were higher than 1 a.u., meaning that the concentrations of the less conjugated molecules were too high to conduct a quantitative study. Despite that, qualitative observations can still be made. The absorption at 220 and 215 nm showed a U-shape curve with a decrease firstly followed by an increase. And those below 210 nm were literally increasing all the way immediately after the illumination was

turned on. This indicates that the more conjugated molecules have been dissociated into less conjugated (and likely in smaller weight) molecules during the photocatalytic treatment, and this process was not completed before 360 min of irradiation. This is in line with the TOC curves that did not show a total mineralization after reaching the same timeline (Figure 5b). In the case of the less efficient self-luminous textile, slow decreases have been observed across all wavelengths, meaning that the conversion of more complex molecules has not generated overconcentrated byproducts that would saturate the active sites of the photocatalysts. These observations are in line with Figure 5c that self-luminous textile led to a relatively less pronounced degradation of pharmaceutical compounds, while the more efficient velvet and the combined systems showed good selectivity on degrading pharmaceutical compounds.

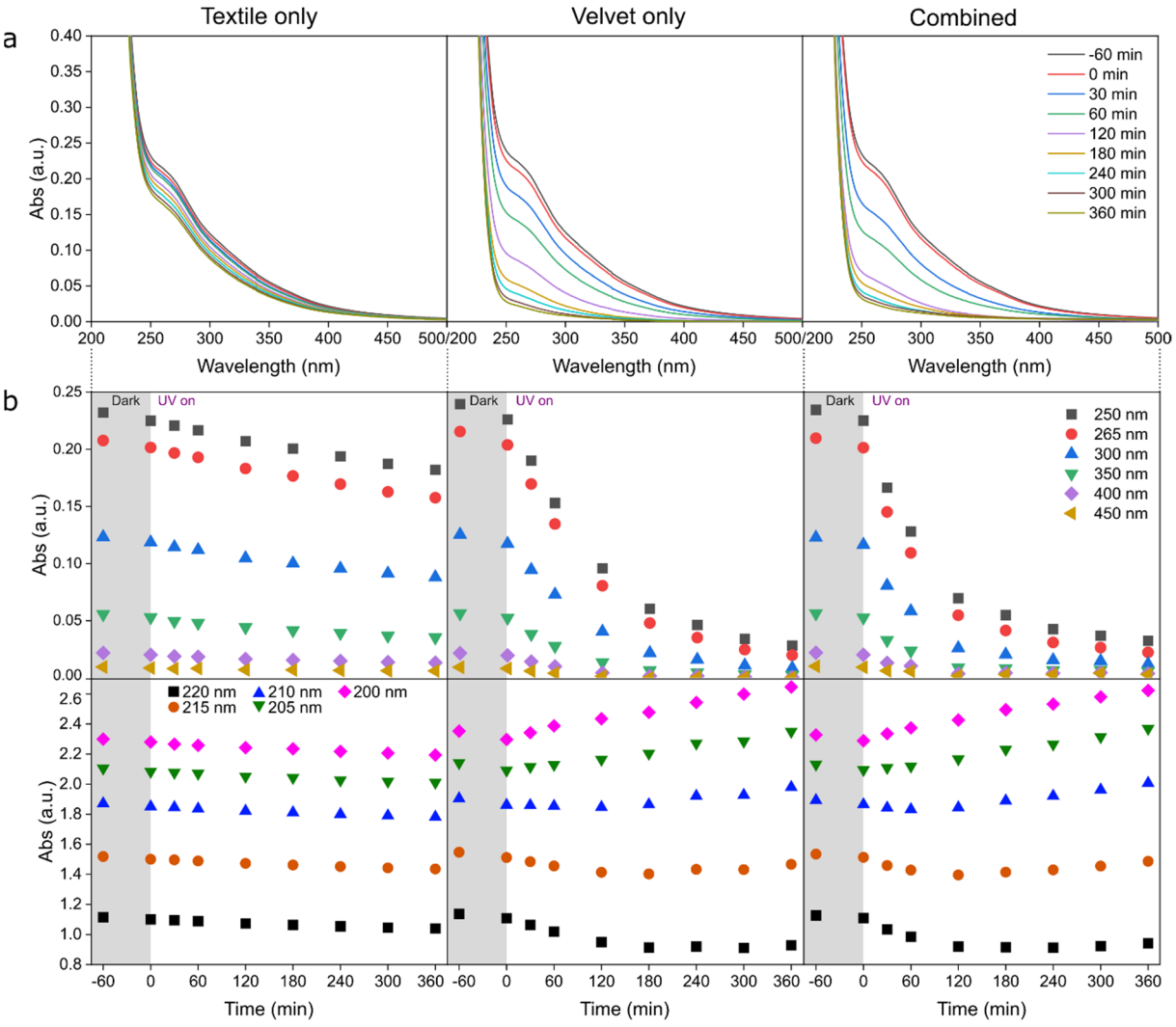

Figure 6. (a) UV-Vis spectra between 200 to 500 nm of the real effluent during the photocatalytic treatment in presence of individual substrates and side-by-side combined system. (b) UV-Vis absorption value at a specific wavelength between 205 to 450 nm of the effluent during the photocatalytic treatment as a function of time in presence of individual substrates and combined system.

Anions in high concentrations were presented in the effluent sample as well (Table S4). Significant presence of chlorides (about 3040 µmol/L) and sulfates (about 690 µmol/L) were particularly evident along with less presences of nitrite, nitrate and phosphates anions. We have only noticed a significant decrease in nitrite concentration in presence of the velvet and the combined system. The decreased amount of nitrite anions corresponded approximately to the increased quantity of nitrate after treatment by the same systems. It could indicate that nitrites were readily oxidized into nitrates by photocatalytic oxidation process. We believe that the generated nitrates likely originated from free nitrites present in the effluent, rather than from the nitrogen contained in the organic molecules. This is because the nitrogen atoms in the latter are primarily in the form of amines, which are typically converted into ammonium ions, as is the case with paracetamol. (Figure 3c). Considering the complicity of chemical environment in the effluent which includes organic molecules and mineral ions, it is more remarkable that the pharmaceutical compounds can be efficiently eliminated by our reactor design.

4. Conclusion

This work has identified two promising substrates for the immobilization of TiO_2 as complementary remediation solution for water treatment, namely a self-luminous textile provided by Brochier® Technologies and a glass fiber velvet provided by Treffler® Production. The glass fiber velvet demonstrated good photocatalytic performance by receiving high irradiation intensity from the external UV lamp, but required large working volume in the reactor. The self-luminous textile suffered from low irradiation intensity delivered by the internal optical fibers but exhibited high flexibility in shape. Subsequently, a side-by-side combination of the above two substrates has been implemented in a horizontal annular flow reactor without the need to expand the reactor volume. The reactor with side-by-side combined substrates has showed more efficiency compared to the individual substrates when accessed for the degradation of phenol, paracetamol in laboratory condition. Finally, by HPLC-MS/MS, ionic chromatography and TOC, the above combined substrates have resulted in a cost-efficient degradation of multiple pharmaceutical compounds (*e.g.*, Caffeine and Gabapentin etc.) in a real effluent sample collected from an urban wastewater treatment plant despite high organic carbon content and elevated inorganic ion concentrations.

Acknowledgements

This work is carried on in the frame of the collaborative international consortium GreenWaterTech financed by the EU and French National Research Agency (ANR) under the ERA-NET Aquatic Pollutants Joint Transnational Call (GA no. 869178). The ERA-NET is an integral part of the activities developed by the Water, Oceans and AMR Joint Programming Initiatives (JPI). Pascale Mascunan and Nicolas Bonnet of IRCELYON are acknowledged for ICP-OES measurements.

Bibliography

[1] O.F.S. Khasawneh, P. Palaniandy, Occurrence and removal of pharmaceuticals in wastewater treatment plants, Process Safety and Environmental Protection 150 (2021) 532-556. https://doi.org/10.1016/j.psep.2021.04.045.

[2] L. Shearer, S. Pap, S.W. Gibb, Removal of pharmaceuticals from wastewater: A review of adsorptive approaches, modelling and mechanisms for metformin and macrolides, Journal of Environmental Chemical Engineering 10(4) (2022) 108106. https://doi.org/10.1016/j.jece.2022.108106.

[3] J.L. Wilkinson, A.B.A. Boxall, D.W. Kolpin, K.M.Y. Leung, R.W.S. Lai, C. Galbán-Malagón, A.D. Adell, J. Mondon, M. Metian, R.A. Marchant, A. Bouzas-Monroy, A. Cuni-Sanchez, A. Coors, P. Carriquiriborde, M. Rojo, C. Gordon, M. Cara, M. Moermond, T. Luarte, V. Petrosyan, Y. Perikhanyan, C.S. Mahon, C.J. McGurk, T. Hofmann, T. Kormoker, V. Iniguez, J. Guzman-Otazo, J.L. Tavares, F. Gildasio De Figueiredo, M.T.P. Razzolini, V. Dougnon, G. Gbaguidi, O. Traoré, J.M. Blais, L.E. Kimpe, M. Wong, D. Wong, R. Ntchantcho, J. Pizarro, G.-G. Ying, C.-E. Chen, M. Páez, J. Martínez-Lara, J.-P. Otamonga, J. Poté, S.A. Ifo, P. Wilson, S. Echeverría-Sáenz, N. Udikovic-Kolic, M. Milakovic, D. Fatta-Kassinos, L. Ioannou-Ttofa, V. Belušová, J. Vymazal, M. Cárdenas-Bustamante, B.A. Kassa, J. Garric, A. Chaumot, P. Gibba, I. Kunchulia, S. Seidensticker, G. Lyberatos, H.P. Halldórsson, M. Melling, T. Shashidhar, M. Lamba, A. Nastiti, A. Supriatin, N. Pourang, A. Abedini, O. Abdullah, S.S. Gharbia, F. Pilla, B. Chefetz, T. Topaz, K.M. Yao, B. Aubakirova, R. Beisenova, L. Olaka, J.K. Mulu, P. Chatanga, V. Ntuli, N.T. Blama, S. Sherif, A.Z. Aris, L.J. Looi, M. Niang, S.T. Traore, R. Oldenkamp, O. Ogunbanwo, M. Ashfaq, M. Iqbal, Z. Abdeen, A. O'Dea, J.M. Morales-Saldaña, M. Custodio, H. de la Cruz, I. Navarrete, F. Carvalho, A.B. Gogra, B.M. Koroma, V. Cerkvenik-Flajs, M. Gombač, M. Thwala, K. Choi, H. Kang, J.L.C. Ladu, A. Rico, P. Amerasinghe, A. Sobek, G. Horlitz, A.K. Zenker, A.C. King, J.-J. Jiang, R. Kariuki, M. Tumbo, U. Tezel, T.T. Onay, J.B. Lejju, Y. Vystavna, Y. Vergeles, H. Heinzen, A. Pérez-Parada, D.B. Sims, M. Figy, D. Good, C. Teta, Pharmaceutical pollution of the world's rivers, Proceedings of the National Academy of Sciences 119(8) (2022) e2113947119. https://doi.org/doi:10.1073/pnas.2113947119.

[4] S. Ustun Odabasi, H. Buyukgungor, Comparative study of degradation of pharmaceutical and personal care products in wastewater by advanced oxidation processes: Fenton, UV/H_2O_2, UV/TiO_2, CLEAN – Soil, Air, Water 52(2) (2024). https://doi.org/10.1002/clen.202300204.

[5] C.V. Rekhate, J.K. Srivastava, Recent advances in ozone-based advanced oxidation processes for treatment of wastewater - A review, Chemical Engineering Journal Advances 3 (2020) 100031. https://doi.org/10.1016/j.ceja.2020.100031.

[6] A. Sharma, M. Yano, C. Zhang, J. Ming, X. Sun, Y. Zhu, G. An, N. Kawazoe, G. Chen, Y. Yang, Efficient and stable immobilization of TiO_2-based composite photocatalytic system for separation and purification of organic pollutants in wastewater under solar light, Journal of Photochemistry and Photobiology A: Chemistry 452 (2024) 115549. https://doi.org/10.1016/j.jphotochem.2024.115549.

[7] A. Duran, J.M. Monteagudo, I. San Martin, Operation costs of the solar photo-catalytic degradation of pharmaceuticals in water: A mini-review, Chemosphere 211 (2018) 482-488. https://doi.org/10.1016/j.chemosphere.2018.07.170.

[8] Y. Feng, H.H.M. Rijnaarts, D. Yntema, Z. Gong, D.D. Dionysiou, Z. Cao, S. Miao, Y. Chen, Y. Ye, Y. Wang, Applications of anodized TiO_2 nanotube arrays on the removal of aqueous contaminants of emerging concern: A review, Water Res. 186 (2020) 116327. https://doi.org/10.1016/j.watres.2020.116327.

[9] N.A. Kouame, D. Robert, V. Keller, N. Keller, C. Pham, P. Nguyen, TiO_2/beta-SiC foam-structured photoreactor for continuous wastewater treatment, Environmental science and pollution research international 19(9) (2012) 3727-34. https://doi.org/10.1007/s11356-011-0719-6.

[10] A.O. Oluwole, E.O. Omotola, O.S. Olatunji, Pharmaceuticals and personal care products in water and wastewater: a review of treatment processes and use of photocatalyst immobilized on functionalized carbon in AOP degradation, BMC chemistry 14(1) (2020) 62. https://doi.org/10.1186/s13065-020-00714-1.

[11] Y. He, N.B. Sutton, H.H.H. Rijnaarts, A.A.M. Langenhoff, Degradation of pharmaceuticals in wastewater using immobilized TiO_2 photocatalysis under simulated solar irradiation, Applied Catalysis B: Environmental 182 (2016) 132-141. https://doi.org/10.1016/j.apcatb.2015.09.015.

[12] B. Erjavec, P. Hudoklin, K. Perc, T. Tišler, M.S. Dolenc, A. Pintar, Glass fiber-supported TiO_2 photocatalyst: Efficient mineralization and removal of toxicity/estrogenicity of bisphenol A and its analogs, Applied Catalysis B: Environmental 183 (2016) 149-158. https://doi.org/10.1016/j.apcatb.2015.10.033.

[13] P. Sun, R. Xue, W. Zhang, I. Zada, Q. Liu, J. Gu, H. Su, Z. Zhang, J. Zhang, D. Zhang, Photocatalyst of organic pollutants decomposition: TiO_2 /glass fiber cloth composites, Catal. Today 274 (2016) 2-7. https://doi.org/10.1016/j.cattod.2016.04.036.

[14] Y. Yan, V. Keller, N. Keller, On the role of $BmimPF_6$ and P/F- containing additives in the sol-gel synthesis of TiO_2 photocatalysts with enhanced activity in the gas phase degradation of methyl ethyl ketone, Applied Catalysis B: Environmental 234 (2018) 56-69. https://doi.org/10.1016/j.apcatb.2018.04.027.

[15] M.M. Rashid, B. Simončič, B. Tomšič, Recent advances in TiO_2-functionalized textile surfaces, Surfaces and Interfaces 22 (2021) 100890. https://doi.org/10.1016/j.surfin.2020.100890.

[16] C. Indermühle, E. Puzenat, F. Dappozze, F. Simonet, L. Lamaa, L. Peruchon, C. Brochier, C. Guillard, Photocatalytic activity of titania deposited on luminous textiles for water treatment, Journal of Photochemistry and Photobiology A: Chemistry 361 (2018) 67-75. https://doi.org/10.1016/j.jphotochem.2018.04.047.

[17] C. Indermühle, E. Puzenat, F. Simonet, L. Peruchon, C. Brochier, C. Guillard, Modelling of UV optical ageing of optical fibre fabric coated with TiO_2, Applied Catalysis B: Environmental 182 (2016) 229-235. https://doi.org/10.1016/j.apcatb.2015.09.037.

[18] Y. Yan, F. Dappozze, L. Khrouz, F.J. López-Tenllado, C. Abdou, C. Prevost, A. Marinas, S. Parola, C. Guillard, Insights into the impact of self-contained sulfur impurity on the superior photocatalytic activity of UV100, J. Catal. 438 (2024) 115704. https://doi.org/10.1016/j.jcat.2024.115704.

[19] K.A. Mohamad Said, A.F. Ismail, Z. Abdul Karim, M.S. Abdullah, A. Hafeez, A review of technologies for the phenolic compounds recovery and phenol removal from wastewater, Process Safety and Environmental Protection 151 (2021) 257-289. https://doi.org/https://doi.org/10.1016/j.psep.2021.05.015.

[20] J.M. Peralta-Hernández, E. Brillas, A critical review over the removal of paracetamol (acetaminophen) from synthetic waters and real wastewaters by direct, hybrid catalytic, and sequential ozonation processes, Chemosphere 313 (2023) 137411. https://doi.org/https://doi.org/10.1016/j.chemosphere.2022.137411.

[21] J.-M. Faurie, D. Chavanon, G. Compigne, E. Periat, Tissu à fils relevés en verre, en quartz ou en métal, 2013.

[22] J.-M. Faurie, D. Chavanon, G. Compigne, E. Periat, Glass, quartz or metal pile fabric, 2015.

[23] J.L. Thomason, Glass fibre sizing: A review, Composites Part A: Applied Science and Manufacturing 127 (2019) 105619. https://doi.org/10.1016/j.compositesa.2019.105619.

[24] C. Brochier, D. Malhomme, E. Deflin, Nappe textile présentant des propriétés dépolluantes par photocatalyse 2007.

[25] C. Brochier, E. Deflin, Complexe éclairant verrier, 2008, pp. 2008-0523.

[26] Y. Huang, S.S. Ho, Y. Lu, R. Niu, L. Xu, J. Cao, S. Lee, Removal of indoor volatile organic compounds via photocatalytic oxidation: A short review and prospect, Molecules 21(1) (2016). https://doi.org/10.3390/molecules21010056.

[27] D.A.H. Hanaor, C.C. Sorrell, Review of the anatase to rutile phase transformation, Journal of Materials Science 46(4) (2011) 855-874. https://doi.org/10.1007/s10853-010-5113-0.

[28] E. R Remesal, Á. Morales-García, F. Illas, Role of n doping in the reduction of titania nanostructures, The Journal of Physical Chemistry C 127(40) (2023) 20128-20136. https://doi.org/10.1021/acs.jpcc.3c04665.

[29] L. Yang, L.E. Yu, M.B. Ray, Photocatalytic oxidation of paracetamol: Dominant reactants, intermediates, and reaction mechanisms, Environmental Science & Technology 43(2) (2009) 460-465. https://doi.org/10.1021/es8020099.